Hindawi
Journal of Chemistry
Volume 2020, Article ID 8690428, 10 pages
https://doi.org/10.1155/2020/8690428

Research Article

Microstructure and Corrosion Behavior of Laser-Cladding CeO_2-Doped Ni-Based Composite Coatings on TC4

Fangxia Ye,[1,2,3] **Wenxuan Shao**,[3] **Xuchao Ye**,[4] **Mingxia Liu**,[1,3] **Yanxiang Xie**,[1,2,3] **Peiying Bian**,[1,2,3] **Xiaoyan Wang**,[1,2,3] **Ling Liu**,[1,3] **and Hong Wu**[5]

[1]*The Key Laboratory for Surface Engineering and Remanufacturing of Shaanxi Province, Xi'an University, Xi'an 710065, China*
[2]*Xi'an Key Laboratory on Intelligent Additive Manufacturing Technologies, Xi'an University, Xi'an 710065, China*
[3]*Shool of Mechanical and Material Engineering, Xi'an University, Xi'an 710065, China*
[4]*Xinjiang Petroleum Engineering Construction Supervision Co., Ltd., Xin Jiang, Kelamayi 834000, China*
[5]*School of Electrical and Mechanical Engineering, Xi'an University of Architecture and Technology, Xi'an 710055, China*

Correspondence should be addressed to Fangxia Ye; 407510325@qq.com

Received 9 June 2020; Accepted 29 June 2020; Published 22 September 2020

Guest Editor: Tifeng Jiao

Laser-cladding CeO_2-doped Ni-based composite coatings were prepared on the surface of a titanium alloy, and the effects of CeO_2 addition on the microstructure, microhardness, and corrosion resistance of the prepared coatings were studied. The results showed that TiC, NiTi, Ni_3Ti, and Ti_2Ni phases were formed on the prepared coatings. Moreover, the addition of CeO_2 in laser-cladding coatings effectively refined the microstructure and reduced the number of cracks generated in the laser-cladding process. When the amount of CeO_2 was 2%, the number of cracks in the laser-cladding coating was significantly reduced compared with that of 0%. When the content of CeO_2 was 2% or 3%, the microhardness of laser-cladding coatings reached the maximum value. At the same time, it was found that the appropriate addition of CeO_2 was helpful to improve the corrosion resistance of the laser-cladding coating. However, excessive CeO_2 addition could reduce the corrosion resistance of the laser-cladding coating.

1. Introduction

Titanium alloys are widely adopted for aerospace, defense, automobile, medical, and other applications due to their low density, high specific strength, good corrosion resistance, and fatigue resistance. Nevertheless, titanium alloys have many limitations, which include a high friction coefficient, weak erosion-corrosion, poor machinability, and relatively poor ability to resist high-temperature oxidation [1, 2]. The limitations have negatively affected the safety and reliability of Ti alloy components and limited their applications. Titanium and its alloys can be corroded in certain environments, especially in environments containing chloride ions. In such environments where the concentration of chloride ion is high, the corrosion attacks will be severe and thus the alloys are corroded. Ti-6Al-4V (TC4) alloy is generally resistant to corrosion, but it can also be rapidly corroded in corrosive environments where the protective oxide layer is destroyed. On the other hand, titanium has a great tendency to react with oxygen. Therefore, it is of importance to protect titanium alloys from corrosion attacks by forming a stable and continuous surface layer.

Different protection approaches such as plasma nitriding [3, 4], physical vapor deposition (PVD) [5–7], chemical vapor deposition (CVD) [8, 9], and plasma spraying process [10, 11] have been applied on Ti-6Al-4V for improving the corrosion resistance. Among these approaches, laser cladding is considered as a promising and effective method because of its large coating thickness, improved compact structure, and excellent performance [12–17]. Also, thanks to the high hardness, good wear resistance, and high-temperature oxidation resistance, Ni-based self-fluxing alloys are widely used in surface-strengthening technologies, such as laser cladding and thermal spraying. As such, this strategy

is often employed not only in academic research but also in industry practice. For instance, it is well known that the laser cladding of Ni-based alloys on the surface of steels can greatly improve the surface properties of the substrate materials. Other representative works are cited in the following. Li et al. [18] fabricated Ni-based composite coatings added with La_2O_3 on carbon steel through laser cladding. Liu et al. [19–21] examined the microstructure and tribological properties of laser-clad Ni-based high-temperature, self-lubricating, and wear-resistant composite coatings. Zhang et al. [22] prepared a Ni60 alloy-cladding layer added with rare earth CeO_2 on the surface of 6063 Al alloys through laser cladding, and they achieved outstanding results. Farahmand et al. [16] investigated the effects of synthesizing a nano-WC powder and rare earth element (RE) on the quality of Ni-WC coatings. Furthermore, they studied the evolution of the molten pool in laser cladding assisted with induction heating and found that the addition of nano-WC particles and La_2O_3 enhanced the coating homogeneity, microstructure refinement, and coating microhardness correspondingly.

This study aims to investigate the effects of CeO_2 amount on the microstructure, microhardness, and corrosion behavior of CeO_2 doped Ni-based composite coatings which are laser cladded on the surface of TC4 alloy in NaCl solutions. In particular, we are interested in knowing if there is an optimal amount of CeO_2 addition in the composite coating. For this purpose, various CeO_2 additions were designed, laser-cladding experiments were carried out, and the obtained coatings were thoroughly evaluated.

2. Experimental Details

The substrate material of this experiment is the TC4 titanium alloy sheet. The chemical composition of TC4 titanium alloy is shown in Table 1. The substrates were prepared from a large TC4 titanium alloy sheet, which was cut to 100 mm × 100 mm × 10 mm by a wire electrical discharge machining (EDM) system. The Ni25 alloy powder and CeO_2 powder with different mass ratios were weighed by a balance. By using a QM3SP04L planetary ball-milling machine, the two powders were mixed and milled to ensure uniformity. The typical physical properties of CeO_2 and the chemical composition of Ni25 are shown in Tables 2 and 3.

Before laser cladding, the surfaces of TC4 substrate plates were cleaned by sandpapers, washed with alcohol, and then dried. An LDM2000 fiber laser processing system was employed for laser cladding, which consists of a 2000W fiber laser system, a powder feeder, and a 3-axis CNC mechanism. Argon gas was used as a protective gas for the cladding operation. The laser-cladding process parameters are listed in Table 4. After cladding, the samples were cut into rectangular specimens of dimensions of 10 mm × 10 mm × 3 mm with the wire EDM system.

The longitudinal section of the specimen was used for characterization. After being well polished with diamond paste and etched with an $HF : NHO_3 : H_2O = 2 : 5 : 43$ solution, the microstructure of the specimen was examined using a scanning electron microscopy (Nova Nano SEM 450) equipped with energy-dispersive X-ray spectroscopy (EDS) unit. The X-ray diffraction (XRD) data were recorded using a PW 1730 X-ray diffractometer (Philips, The Netherlands) with monochromated Cu Kα radiation at 40 kV and 40 mA in the 2θ range of 10–90°. Microhardness of the specimen was measured by using an HDX-1000 digital microhardness tester (Taiming Test Co., China), which consists of a square-based pyramidal diamond indenter with a 136° angle between two opposite faces. The static load applied was 50 g and the dwell time of loading was 15 sec. An average value of microhardness was taken from at least five different measurements. Immersion corrosion analysis was carried out using a CS310H electrochemical workstation. The 3.5% NaCl solution was chosen as the immersion medium and its pH was maintained at 6.5.

The corrosion resistance of the laser-cladding coatings was tested using an electrochemical work station. At the beginning of the experiment, the surface of each sample was polished with sandpapers and then wrapped with copper wire of 1 mm in diameter. The other exposed areas of the sample were sealed with 703 silicone rubber, and only a cylindrical surface of Φ6 mm was left on the surface of the sample. The sample was the working electrode, the saturated Mercury electrode was used as the reference electrode, the metal platinum sheet was used as the auxiliary electrode, and the reference electrode and the research electrode were connected by a salt bridge. A sodium chloride solution with a mass fraction of 3.5% was used as a reaction solution. The dynamic potential scan was performed at a scanning speed of 1 mV/s, and the scanning range was −1 V to +1.5 V.

3. Results and Discussion

Figure 1 shows the X-ray diffraction spectrum of laser-cladding coatings with different CeO_2 contents. The XRD result indicates that TiC, NiTi, Ni_3Ti, and Ti_2Ni exist in the laser-cladding coatings. It can be observed that the higher content of CeO_2 leads to the stronger the Ti_2Ni diffraction peaks. However, the types of other phases are not changed.

Figure 2 presents the macromorphology of coatings with different CeO_2 contents. It can be seen that there are no visible defects, such as lack of fusion and porosity, in the laser-cladding coatings. The number of cracks in the laser-cladding coatings varies with the rare earth CeO_2 content. When the content of CeO_2 is less than 2%, it can effectively reduce the crack generation of the laser-cladding coatings. When the content of CeO_2 is more than 2%, the number of cracks begins to increase again. As such, the proper amount of rare earth CeO_2 can effectively inhibit the laser-cladding cracks, and the excessive amount of rare earth CeO_2 can increase the number of laser-cladding cracks. The reason can be illustrated as follows. The addition of rare earth elements in the laser-cladding process can effectively refine the structure and increase the grain boundary. The crack propagation in the laser-cladding coatings is hindered and further reduces the harmful effect on the substances. All these lead to the improvement of strength and toughness of the laser-cladding coatings.

Table 1: The chemical composition of TC4 titanium alloy (wt.%).

Elements	Al	V	Fe	C	N	H	O	Ti
Wt.%	5.5 ~ 6.8	3.5 ~ 4.5	≤0.3	≤0.1	≤0.05	≤0.01	≤0.02	Balance

Table 2: The physical performance of CeO_2.

Melting point (°C)	Specific gravity ($g \cdot cm^{-2}$)	Color	Heat of formation ($kJ^{\circ}mol^{-1}$)	Free energy ($kJ \cdot mol^{-1}$)	Enthalpy change ($kJ \cdot mol^{-1}$)	Purity (%)
1965	7.13	Yellow and white	−2596.65	−1025.35	62.34	99.99

Table 3: The chemical composition of Ni25 (wt.%).

	C	B	Si	Cr	Fe	Ni	HRC
Ni25	≤0.2	1.0~2.0	2.0~3.5	5.0~10.0	≤4	Balance	20~30

Table 4: Specimen numbers and corresponding laser-cladding process parameters and CeO_2 contents.

Specimen number	S0	S1	S2	S3	S4	S5	S6
Laser power (kW)	1	1	1	1	1	1	1
Laser scanning rate ($mm \cdot min^{-1}$)	600	600	600	600	600	600	600
Powder feeding rate ($g \cdot min^{-1}$)	8	8	8	8	8	8	8
Argon gas velocity ($L \cdot min^{-1}$)	15	15	15	15	15	15	15
Spot diameter (mm)	3	3	3	3	3	3	3
CeO_2 (wt.%)	0	1	2	3	4	5	6

Figure 3 shows the SEM photographs of the laser-cladding coatings for different CeO_2 contents. As it can be seen from Figure 3(a), the dendritic structures of the Ni25 cladding layers are coarse, and many grain segregations, accompanied by a large number of pores, can be observed in the local area, whereas the Ni25-cladding layers added with rare earth oxides exhibit compact dendritic structures, and the grains are refined. This finding agrees with the existing related studies [23, 24]. This phenomenon can be attributed to the improved liquidity of the molten pool as a result of the addition of rare earth oxides, which is beneficial for gas discharge from the molten pool. Consequently, the pores and cracks in the cladding layers are eliminated. Nevertheless, the degree of rare earth refinement is not unlimited. When the content of rare earth CeO_2 is more than 2%, the microstructure of the laser-cladding coatings becomes coarser. In particular, the size of dendrite in the laser-cladding coatings increases significantly. Thus, it can be seen that there is an optimum value for the content of the rare earth in the process of refining the microstructure of the laser-cladding coatings. It can be illustrated as follows. Firstly, when the rare earth element is segregated in the grain boundary due to its adsorptivity, it can block the growth of the grain and reduce the grain boundary. At the same time, the driving force of the grain growth is reduced and the microstructure is refined [25]. Secondly, according to the analysis of physical and chemical aspects, the contradiction exists in the solid-liquid system after the formation of the crystal nucleus. In the temperature below the freezing point, the formation of the crystal nucleus will bring about a free enthalpy reduction of the system which is the driving force of the nucleation. Moreover, the generated crystal nuclei are small and the degree of dispersion is high, which causes an increase in free enthalpy and resists the nucleation. It can be seen that the free enthalpy of the new grain boundaries plays an important role in the formation and development of crystal nuclei. With the increase of nucleation radius r, the free enthalpy ΔG of the whole solid-liquid system undergoes a process of rising first and then decreasing. Therefore, there exists a maximum value, which is the critical nucleation work. At this time, the nucleation radius of the whole solid-liquid system should be the critical radius r_k, and r_k equation is calculated as $r_k = 2\sigma/\Delta G$, in which σ is the surface tension on solid-liquid interface and Δg is the free volume change of unit volume.

Because of the strong electronegativity and active chemical properties of Ce atom, it is easy to fill the surface defects of alloy phase in liquid metal, so that the surface tension on the interface between the two phases is low. Based on r_k equation, it is understandable that the critical radius of the nucleus reduces after the reduction of surface tension, and the number of effective nucleation increases. As a result, the refinement of the microstructure can be achieved.

Figure 4 illustrates the point spectrum analysis of the cross section of sample S2, and it can be seen that the main elements in the coating are C, Ti, and Ni, and the atomic ratio of C and Ti is close to 1 : 1. Furthermore, the results of line scanning analysis from the substrate to the coating of sample S2 are shown in Figure 5. It can be seen that there are mainly Ti, Ni, C, and other elements in the coating. The Ni elements are mainly distributed in the coating layer, the Ti elements are distributed in the coating and the matrix, and the content in the substrate is higher. Other elements are distributed uniformly in the coating and the substrate, which indicates that the rare earth CeO_2 is diffused into the substrate, and a metallurgical bond is developed between the coating and the substrate.

Figure 6 shows the microhardness distribution curves of laser-cladding coatings with various CeO_2 contents. It can be seen that the curves follow a similar trend in which the microhardness is higher in the cladding layer and much lower in the substrate. More importantly, the hardness of cladding coatings appears to be different with various additions of CeO_2. When the addition of CeO_2 is at 0% and 1%, the maximum microhardness of cladding coatings is below $750HV_{0.05}$. When the amount of the rare earth CeO_2 is 2%

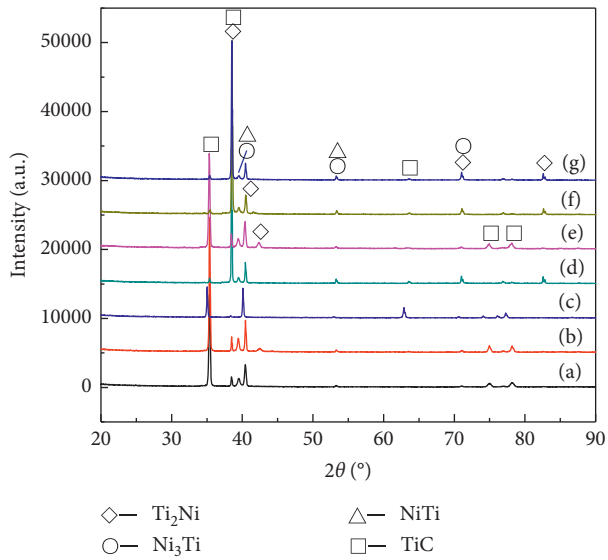

Figure 1: X-ray diffraction spectrum of laser-cladding coatings with different CeO_2 contents: (a) 0%, (b) 1%, (c) 2%, (d) 3%, (e) 4%, (f) 5%, and (g) 6%.

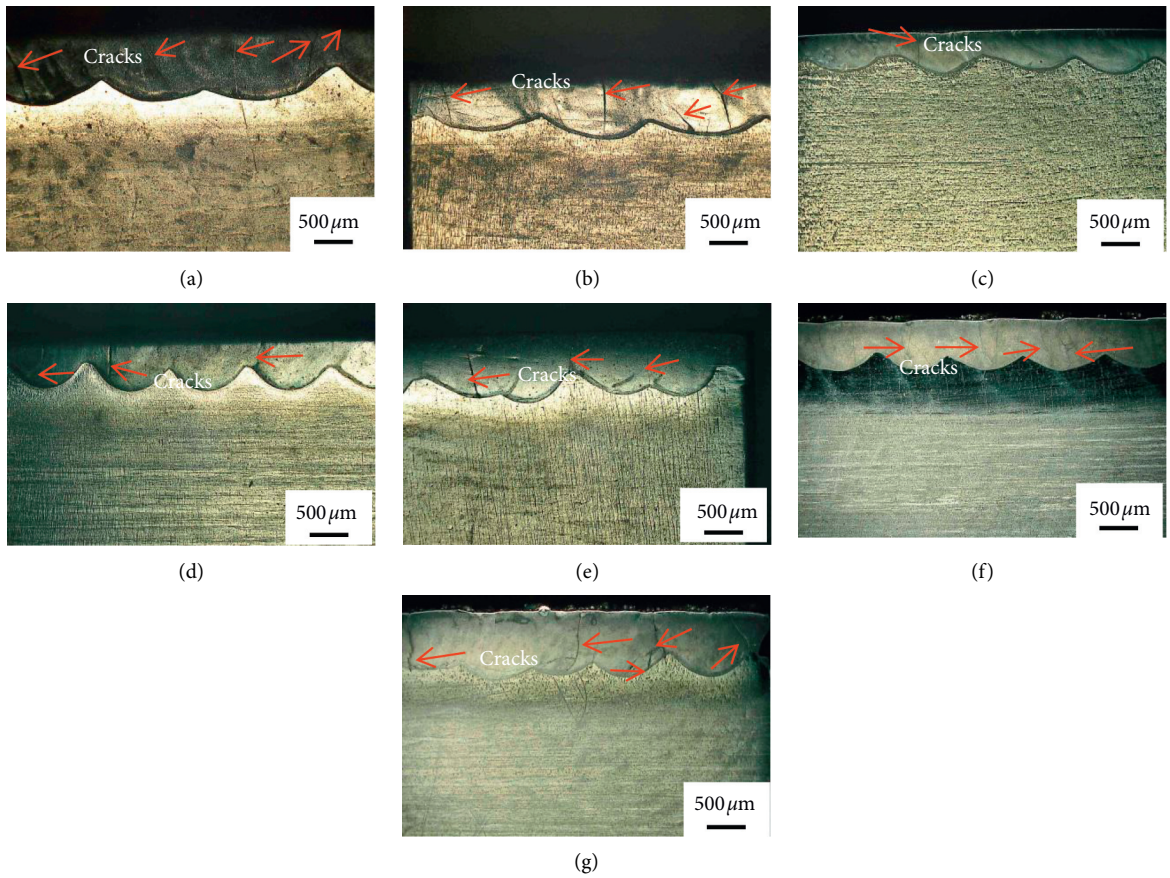

Figure 2: The macromorphology of the coatings with different CeO_2 contents: (a) 0%, (b) 1%, (c) 2%, (d) 3%, (e) 4%, (f) 5%, and (g) 6%.

and 3%, the maximum microhardness of cladding coatings exceeds $900HV_{0.05}$. The microhardness increase is expected in that the microstructure of the cladding layer is refined by the addition of rare earth elements. The rare earth oxide is dissolved in the solid solution and acts as a solid solution strengthening agent. The laser-cladding process is a non-equilibrium process, and it is possible to obtain the supersaturated solid solution of the rare earth element. The

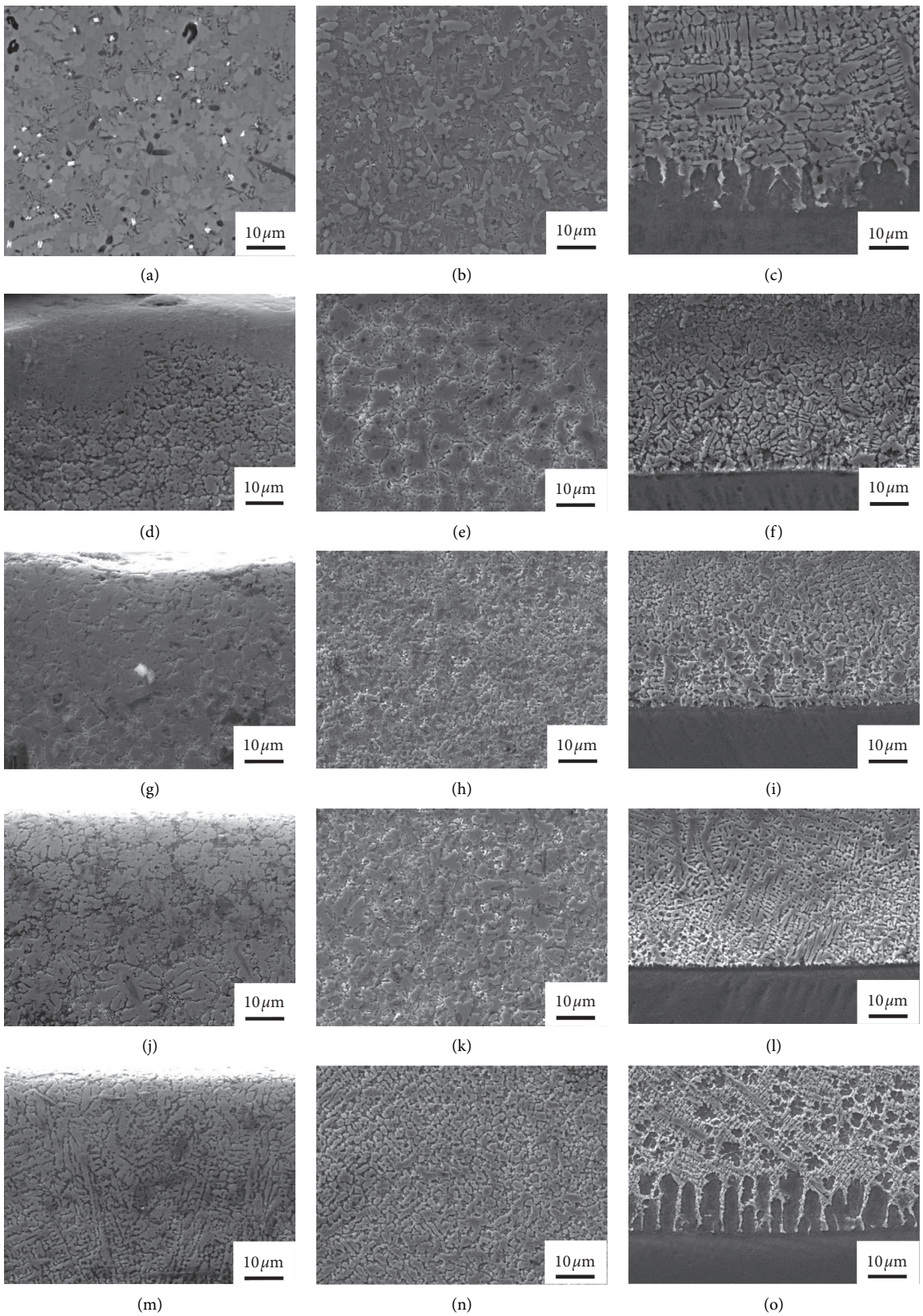

Figure 3: Continued.

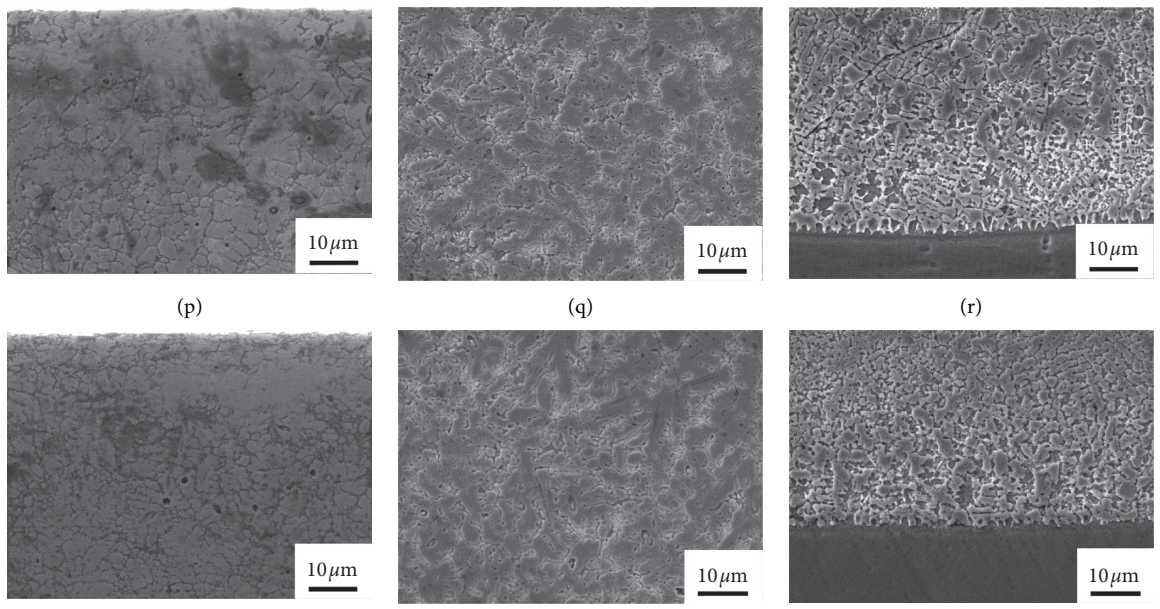

Figure 3: The SEM photographs of the laser-cladding coatings for different CeO_2 contents: (a–c) 0%, (d–f) 1%, (g–i) 2%, (j–l) 3%, (m–o) 4%, (p–r) 5%, and (s–u) 6%. (a, d, g, j, m, p, and s) The surface portion of coatings. (b, e, h, k, n, q, and t) The middle portion of coatings. (c, f, i, l, o, r, and u) The surface portion of coatings.

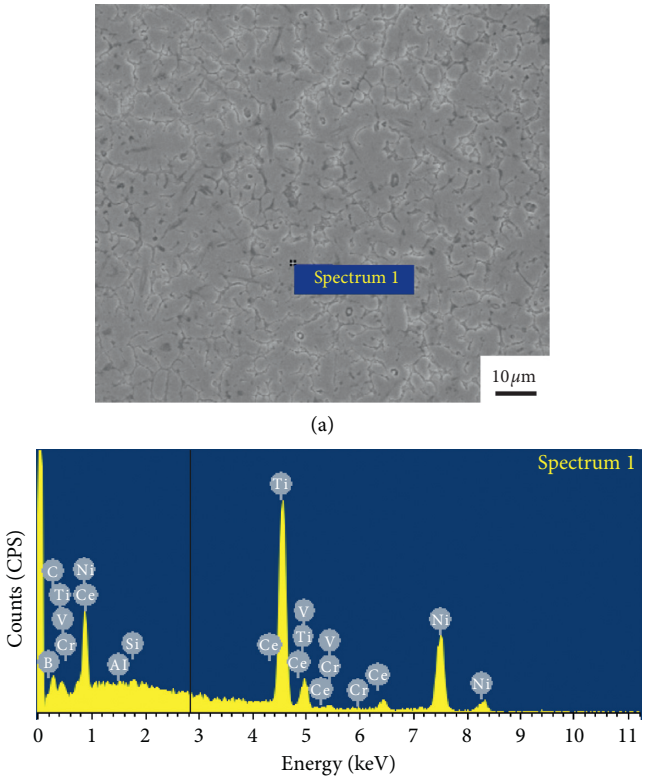

Elements	BK	CK	Al K	Si K	Ti K	V K	Cr K	Ni K	Ce L	Total
Wt. %	2.12	10.17	0.21	1.13	27.95	0.15	1.17	56.33	0.77	100.00
At. %	7.36	31.77	0.29	1.50	21.90	0.11	0.85	36.01	0.21	100.0

(c)

Figure 4: The point spectrum analysis of the cross section of sample S2: (a) the cross section of the S2 coating, (b) elements distribution of coating, and (c) the atomic ratio of elements.

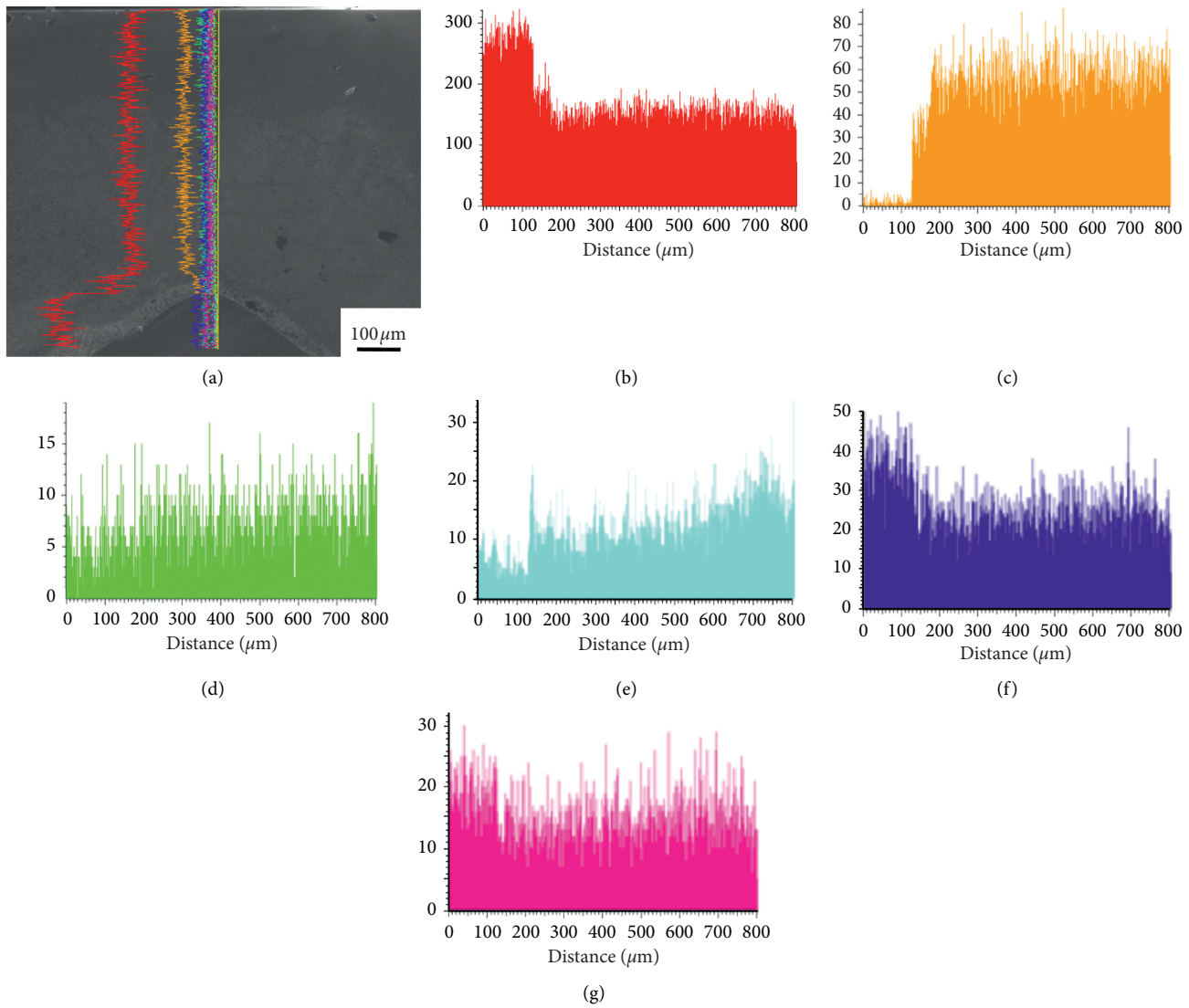

Figure 5: The results of line scanning analysis from the substrate to the coating of sample S2: (a) line scan image; (b) Ti element, (c) Ni element, (d) B element, (e) C element, (f) V element, and (g) Ce element.

formation of the solid solution will produce strong lattice distortion, resulting in significant solid solution strengthening. Nevertheless, with the further increase of CeO_2 content, the microhardness of the cladding layer gradually decreases because the excessive addition of rare earth oxides is easy to form internal inclusions with other components, which in turn decreases the density and the microhardness of the laser-cladding coating.

It can be seen from the above analysis that the amount of rare earth CeO_2 addition influences the phase composition, microstructure, density of cracks, and microhardness of the cladding coating. It is thus intuitive that the rare earth CeO_2 addition may have an effect on the corrosion resistance of the laser-cladding coating. The corrosion resistance of the laser-cladding coating with different contents of CeO_2 is obtained by an electrochemical work station.

Figure 7 shows the potentiodynamic polarization curves of samples added with different CeO_2 contents in 3.5% NaCl solution. For each sample, the test result consists of a cathode polarization curve and an anode polarization curve. The cathode polarization curves remain unchanged in the experiment, which means that none of all the cathode polarization processes are changed. With the increase of voltage, the anodizing starts to occur. It can be seen from the diagram that the self-corrosion potential of the sample with CeO_2 content of 2% is −0.15 V, which is much higher than that (−0.30 V) of the sample with rare earth content of 0%.

It shows that the addition of the proper amount of rare earth can improve the corrosion resistance of the laser-cladding coating. However, with the CeO_2 content higher than 3%, the corrosion potential decreases again. In particular, the corrosion potential of the coating decreases from −0.2 V (with 3% CeO_2) to −0.45 V (with 6% CeO_2). This is because the grains in the coating will be refined obviously when the amount of CeO_2 is moderate. With the increase of the number of crystals, the segregation of components can

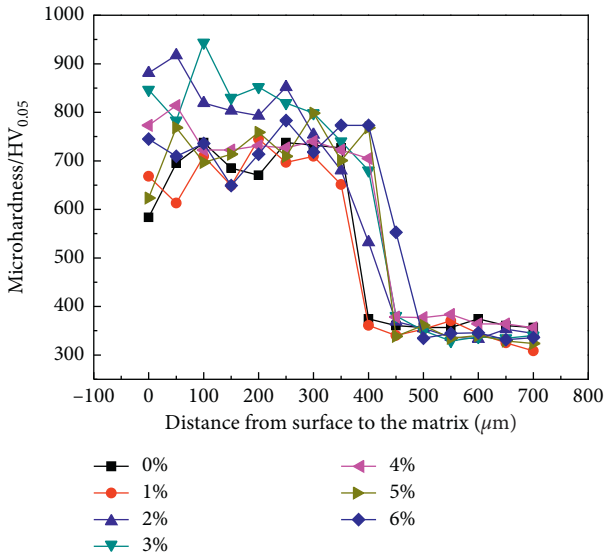

Figure 6: The microhardness distribution curves of laser-cladding coatings with various CeO_2 contents.

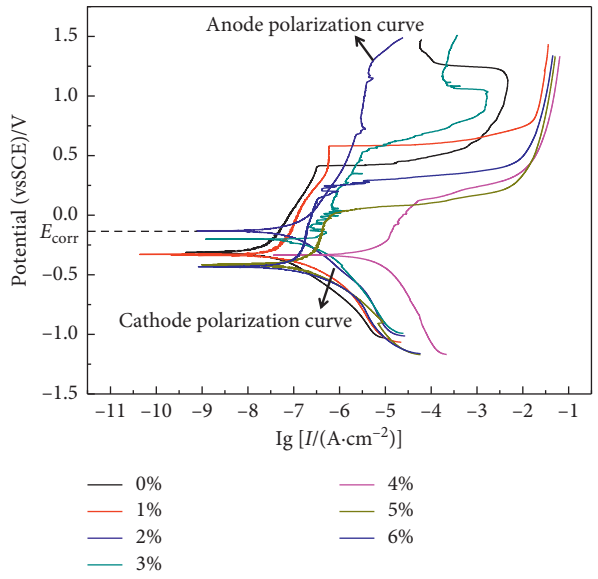

Figure 7: The potentiodynamic polarization curves of samples added with different CeO_2 contents in 3.5% NaCl solution.

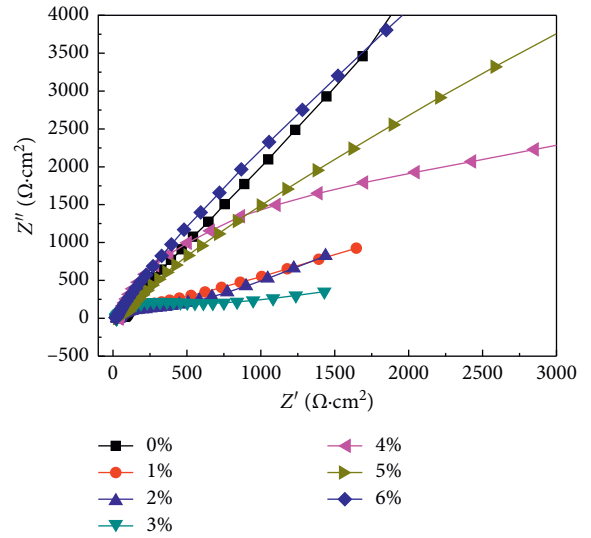

Figure 8: Nyquist plot of the laser-cladding coating with different CeO_2 contents in 3.5% NaCl solution.

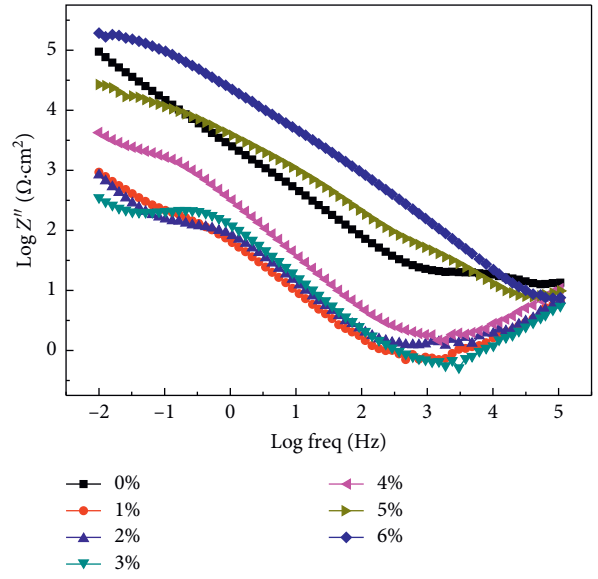

Figure 9: Bode plot of the laser-cladding coatings with different CeO_2 contents in 3.5% NaCl solution.

be improved and the grain boundary can be prolonged, so the impurity density and the corrosion tendency at the grain boundary are reduced.

Figure 8 shows the Nyquist plot of the laser-cladding coating with different CeO_2 contents in a 3.5% NaCl solution. It can be seen that the diameter of the capacitive reactance circle in the Nyquist diagram is small, indicating that the laser-cladding coating is excellent in corrosion resistance in the high-frequency region. The Nyquist image is equivalent to a straight line at this time, indicating that the cladding layer is equivalent to an insulating layer with a large capacitance value and a small resistance value, which can effectively protect the titanium alloy substrate from corrosion. Moreover, the linear slope of 2% CeO_2 content is the largest, indicating that the corrosion resistance of the laser-cladding coating is the best when the rare earth content is 2%.

Figure 9 shows the bode plot of the laser-cladding coatings with different CeO_2 contents in a 3.5% NaCl solution. It can be seen that the high-frequency impedance increases with the increase of CeO_2 content, while the low-frequency impedance firstly increases and then decreases with the increase of CeO_2 content. The reduction of the low-frequency impedance means the decrease of the solution resistance, and the increase of the high-frequency impedance indicates that the grains in the coatings will be refined when the amount of CeO_2 is at a proper level.

4. Conclusions

In conclusion, this study shows that doping the Ni-alloy coatings with CeO_2 could change the microstructure and properties of the Ni-alloy coatings. The XRD result indicates that TiC, NiTi, Ni_3Ti, and Ti_2Ni phases exist in the laser-cladding coatings. The phase composition of the coatings does not change with the increase of CeO_2 content up to 6%. The microstructure of the sample with CeO_2 content of 2% is significantly refined, because the Ce atom reduces the critical radius of the crystal nucleus and the number of effective nucleus increases. When the rare earth addition exceeds the critical value, grain refinement effect starts to deteriorate, and the grains become coarser. The addition of CeO_2 can increase the microhardness of the coating. With 2% CeO_2, the maximum microhardness of the coating reaches over 900 $HV_{0.05}$, while that of coating with 0% CeO_2 is below $750HV_{0.05}$. The addition of the proper amount of rare earth can significantly improve the corrosion resistance of the laser-cladding coating. This is because the grains in the coatings will be refined when the amount of CeO_2 is at a proper level.

Data Availability

The data used to support the findings of this study are included within the supplementary information files.

Conflicts of Interest

The authors declare that they have no conflicts of interest.

Acknowledgments

The authors (Ye, Shao, Xie, Bian, Wang, Liu, and Wu) are grateful for financial support from the Shaanxi Provincial Natural Science Foundation Project (2019JQ-891 and 2020JQ-889), Xi'an Science and Technology Plan Project (2020KJWL01), the Science Foundation of Shaanxi Provincial Department of Education (20JS133), the National Innovation and Entrepreneurship Training Program for College Students (DC2020022), the Special Research Project of Shaanxi Provincial Department of Education (19JK0739), the research team of advanced surface engineering and equipment life extension of Xi'an University (XAWL-KYTD013) the General Projects in the Industrial Field of Shaanxi Provincial Science and Technology Department (2020GY-193), and the Science Foundation of Shaanxi Provincial Department of Education (15JS054).

References

[1] M. Nabhani, R. Shoja Razavi, and M. Barekat, "Corrosion study of laser cladded Ti-6Al-4V alloy in different corrosive environments," *Engineering Failure Analysis*, vol. 97, pp. 234–241, 2019.

[2] D. Nam, J. Do, and S. Lee, "Microstructure and corrosion behaviour of laser-cladding Al-Ni-TiC-CeO_2 composite coatings on S355 offshore steel," *Journal of Alloys and Compounds*, vol. 770, pp. 771–783, 2019.

[3] O. Unal, E. Maleki, and R. Varol, "Effect of severe shot peening and ultra-low temperature plasma nitriding on Ti-6Al-4V alloy," *Vacuum*, vol. 150, pp. 69–78, 2018.

[4] T. T. Peng, X. B. Zhao, Y. Chen, L. Tang, K. X. Wei, and J. Hu, "Improvement of stamping performance of H13 steel by compound-layer free plasma nitriding," *Surface Engineering*, vol. 36, no. 5, pp. 492–497, 2019.

[5] C. Song, M. Liu, Z.-Q. Deng, S.-P. Niu, C.-M. Deng, and H.-L. Liao, "A novel method for in-situ synthesized TiN coatings by plasma spray-physical vapor deposition," *Materials Letters*, vol. 217, pp. 127–130, 2018.

[6] E. Marin, R. Offoiach, A. Lanzutti, M. Regis, S. Fusi, and L. Fedrizzi, "Hybrid diffusive/PVD treatments to improve the tribological resistance of Ti-6Al-4V," *Bio-medical Materials and Engineering*, vol. 24, no. 1, pp. 581–592, 2014.

[7] V. V. Sáenz, M. G. Barandika, G. U. Ruizde et al., "Characterization of Ti-C-N coatings deposited on Ti6Al4V for biomedical applications," *Journal of Inorganic Biochemistry*, vol. 117, pp. 359–366, 2012.

[8] A. Reina, X. Jia, J. Ho et al., "Large area, few-layer graphene films on arbitrary substrates by chemical vapor deposition," *Nano Letters*, vol. 9, no. 1, pp. 30–35, 2009.

[9] S. Chaitoglou and E. Bertran, "Effect of temperature on graphene grown by chemical vapor deposition," *Journal of Materials Science*, vol. 52, no. 13, pp. 8348–8356, 2017.

[10] K. A. Khor, Y. W. Gu, C. H. Quek, and P. Cheang, "Plasma spraying of functionally graded hydroxyapatite/Ti-6Al-4V coatings," *Surface & Coatings Technology*, vol. 168, no. 2-3, pp. 195–201, 2003.

[11] T. Valente and C. Bartuli, "A plasma spray process for the manufacture of long-fiber reinforced Ti-6Al-4V composite monotapes," *Journal of Thermal Spray Technology*, vol. 3, no. 1, pp. 63–68, 1994.

[12] Y.-F. Liu, Y.-L. Zhou, Q. Zhang, F. Pu, R.-H. Li, and S.-Z. Yang, "Microstructure and dry sliding wear behavior of plasma transferred arc clad Ti5Si3 reinforced intermetallic composite coatings," *Journal of Alloys and Compounds*, vol. 591, no. 13, pp. 251–258, 2014.

[13] X. Nie, W. He, S. Zang, X. Wang, and J. Zhao, "Effect study and application to improve high cycle fatigue resistance of TC11 titanium alloy by laser shock peening with multiple impacts," *Surface and Coatings Technology*, vol. 253, pp. 68–75, 2014.

[14] F. Weng, H. Yu, C. Chen et al., "Effect of process parameters on the microstructure evolution and wear property of the laser cladding coatings on Ti-6Al-4V alloy," *Journal of Alloys and Compounds*, vol. 692, pp. 989–996, 2017.

[15] C. Tan, H. Zhu, T. Kuang, J. Shi, H. Liu, and Z. Liu, "Laser cladding Al-based amorphous-nanocrystalline composite coatings on AZ80 magnesium alloy under water cooling condition," *Journal of Alloys and Compounds*, vol. 690, pp. 108–115, 2017.

[16] P. Farahmand, S. Liu, Z. Zhang, and R. Kovacevic, "Laser cladding assisted by induction heating of Ni-WC composite enhanced by nano-WC and La_2O_3," *Ceramics International*, vol. 40, no. 10, pp. 15421–15438, 2014.

[17] M. Z. Mehrizi, M. Shamanian, A. Saidi, R. Shoja-Razazvi, and R. Beigi, "Evaluation of oxidation behavior of laser clad CoWSi-WSi_2 coating on pure Ni substrate at different temperatures," *Ceramics International*, vol. 41, no. 8, pp. 9715–9721, 2015.

[18] M. Li, B. Han, Y. Wang, and K. Pu, "Effects of La_2O_3 on the microstructure and property of laser cladding Ni-based ceramic coating," *Optik*, vol. 130, pp. 1032–1037, 2017.

[19] X.-B. Liu, X.-J. Meng, H.-Q. Liu et al., "Development and characterization of laser clad high temperature self-lubricating wear resistant composite coatings on Ti-6Al-4V alloy," *Materials & Design*, vol. 55, pp. 404–409, 2014.

[20] X.-B. Liu, H.-Q. Liu, X.-J. Meng et al., "Effects of aging treatment on microstructure and tribological properties of nickel-based high-temperature self-lubrication wear resistant composite coatings by laser cladding," *Materials Chemistry and Physics*, vol. 143, no. 2, pp. 616–621, 2014.

[21] X.-B. Liu, C. Zheng, Y.-F. Liu et al., "A comparative study of laser cladding high temperature wear-resistant composite coating with the addition of self-lubricating WS2 and WS2/(Ni-P) encapsulation," *Journal of Materials Processing Technology*, vol. 213, no. 1, pp. 51–58, 2013.

[22] G. Zhang, C. Wang, and Y. Gao, "Mechanism of rare earth CeO_2 on the Ni-based laser cladding layer of 6063 Al surface," *Rare Metal Materials and Engineering*, vol. 45, no. 4, pp. 1002–1006, 2016.

[23] C. Wang, Y. Gao, R. Wang, D. Wei, M. Cai, and Y. Fu, "Microstructure of laser-clad Ni60 cladding layers added with different amounts of rare-earth oxides on 6063 Al alloys," *Journal of Alloys and Compounds*, vol. 740, pp. 1099–1107, 2018.

[24] X. He, R. G. Song, and D. J. Kong, "Microstructure and corrosion behaviour of laser-cladding Al-Ni-TiC-CeO_2 composite coatings on S355 offshore steel," *Journal of Alloys and Compounds*, vol. 770, pp. 771–783, 2019.

[25] S. G. Chen, X. M. Zhang, Q. C. Zheng, and R. F. Li, "Effect of CeO_2 on microstructure and properties of Ni60 alloy coating by laser cladding," *Laser Technology*, vol. 41, pp. 904–908, 2017.